Manuscript

Click here to download Manuscript Manuscript-YM-RT-PL-JL-2017-02-07F.docx

A New Simplified Method for Designing Seismically Isolated Highway Bridges with Massive Piers

Yudong Mao[1], Robert Tremblay[2], Pierre Léger[3] and Jianzhong Li[4]

[1]Ph.D. Candidate, State Key Laboratory of Disaster Reduction in Civil Engineering, Tongji Univ., Shanghai 200092, China; presently, Visiting Researcher, Dept. of Civil, Geological, and Mining Engineering, Polytechnique Montréal, Montréal, QC H3C 3A7, Canada. E-mail: 1310200@tongji.edu.cn

[2]Professor, Dept. of Civil, Geological, and Mining Engineering, Polytechnique Montréal, Montréal, QC H3C 3A7, Canada. E-mail: robert.tremblay@polymtl.ca

[3]Professor, Dept. of Civil, Geological, and Mining Engineering, Polytechnique Montréal, Montréal, QC H3C 3A7, Canada. E-mail: pierre.leger@polymtl.ca

[4]Professor, State Key Laboratory of Disaster Reduction in Civil Engineering, Tongji Univ., Shanghai 200092, China. E-mail: lijianzh@tongji.edu.cn

Abstract

This paper proposes two new models for the simplified seismic analysis of seismically isolated highway bridges with massive piers. Both models include two components: one of which includes the superstructure mass, the isolators and massless pier, and the other one the pier with its distributed mass and stiffness properties. In one model, the isolator stiffness is added at the top of the pier in the second component. The total seismic response is obtained from the square root of the sum of squares (SRSS) of the two individual component results. Applicability and accuracy of the models are assessed by considering bridges with wide ranges of stiffness and mass properties of piers, M_p, and superstructures, M_{ss}. Multimode Spectral Analysis (MMSA) and Nonlinear Time History Analysis (NLTHA) are used to define reference solutions for the superstructure displacements, vibration periods, and shears and moments at pier bases. Results from four currently available models including the model prescribed in AASHTO and CAN/CSA S6-14 codes are also examined. The study shows that current models for the simplified analysis method yield good estimates of superstructure displacements and vibration periods; however, they generally underestimate the shear and moment demands at pier bases. The errors are more significant for more massive piers or when the stiffness of the piers is high compared to that of the isolators. In contrast, for all bridges studied, the seismic responses from the proposed models show very good agreement with those from the MMSA. Better predictions

are obtained when considering the isolator stiffness in the second component of the model. The NLTHA results also show that the proposed models give overall satisfactory predictions for pier base shears and moments. The proposed models extend the range of application of the AASHTO and CAN/CSA S6-14 simplified method to isolated bridges with massive piers, while preserving its simplicity with limited extra computational effort.

Keywords: *Highway bridges; Seismic isolation design; Massive piers; Simplified method; Multimodal analysis; Nonlinear time history analysis*

Introduction

Seismic isolation, i.e., decoupling the structure from the ground, provides an effective passive method of protecting structures against severe seismic events. Because most isolation systems are nonlinear, it initially appears that only nonlinear analysis methods can be used in their design, such as a nonlinear time-history analysis (NLTHA). However, if the nonlinear properties can be linearized, equivalent linear (elastic) methods may be used, in which case many methods are suitable for the design and analysis of isolated bridges (Buckle et al. 2006; Constantinou et al. 2011; AASHTO 2014; CSA 2014; FHWA 2014). Simplified analysis methods often use a single-degree-of-freedom (SDOF) system with effective linear (elastic) and equivalent viscous properties to predict the displacement demand directly from prescribed response spectra (Hwang et al. 1997; Guyader and Iwan 2006; Feng and Lee 2009). Using fundamental assumptions, such as those of effective linear springs and equivalent viscous damping, and neglecting pier mass contributions, simplified methods can give satisfactory results for regular isolated bridges (e.g., bridges with small mass piers with approximately straight continuous decks in the longitudinal direction and no abrupt changes in weight, stiffness or geometry, or with simply supported decks with no significant interaction between piers; Dicleli et al. 2005; Jara and Casas 2006; Cardone et al. 2009; Jara et al. 2012). They are conceptually simple and easy to apply because the dynamic response of the substructure is ignored. While not necessarily the most accurate, they are particularly useful in preliminary design or when verifying the feasibility of seismic isolation for a particular bridge. They are therefore generally the starting point in seismic isolation design, followed by more rigorous methods as the bridge design progresses. These simplified analysis methods have been adopted in AASHTO Guide Specifications for Seismic Isolation Design (AASHTO 2014) and CAN/CSA S6-14 Canadian Highway Bridge Design Code (CSA 2014) used in North America.

In seismic isolation, the substructure is not isolated from ground motions but is decoupled from the relatively larger mass of the superstructure (Priestley et al. 1996). Therefore, neglecting or approximating the effect of pier masses may lead

to a serious underestimation of the total base shears of massive piers, which may be approximately 50% less than the actual seismic force (Reinhorn et al. 1998; Franchin et al. 2001; Buckle et al. 2011). A number of studies have been conducted to extend the application of the simplified methods to a broader range of bridges, and new solutions are continuously being proposed and investigated (Tsopelas et al. 1997; Fadi and Constantinou 2010; Ozdemir and Constantinou 2010; Wei and Buckle 2012; Wei et al. 2013; Al-Ani and Singh 2014). Among these studies, some assumptions are commonly used for the case of bridges with heavy piers, such as modeling a certain percentage of individual pier masses M_p (generally 1/3rd of the total pier masses) and the tributary superstructure mass M_{ss} lumped at the pier top, with the rest of the pier assumed massless. The approach is applied in the design examples included in AASHTO (2014). This assumption is valid for short- to moderate-span isolated bridges, but may exhibit significant limitations for long-span bridges with M_p/M_{ss} ratios above 0.2 (Franchin et al. 2001; Adhikari 2010; Wei et al. 2013).

This paper proposes an alternative approach in which isolated highway bridges are analyzed as two components with or without interactions. One component includes the superstructure mass, and the other includes the pier masses. The seismic response of the total system is obtained from the square root of the sum of squares (SRSS) of the individual component results. The proposed simplified method considers the actual pier mass and stiffness distributions rather than using a portion of the pier masses as the participating masses. The intent is to extend the range of application of the AASHTO and CAN/CSA S6-14 simplified methods to isolated bridges with massive piers while preserving its simplicity without significant additional computational effort. Time history analysis (THA), multimode spectral analysis (MMSA) and current simplified analysis methods (SM) are first briefly reviewed and compared. The new simplified method is introduced and described. It is shown that the proposed simplified method could be declined in two variants (later labeled E and F in the paper) with progressive modelling refinements to improve accuracy. The proposed simplified method is validated against the results from multimode spectral analysis for a regular 4-span bridge with various substructure mass and stiffness ratios and a 5-span bridge with heavy non-uniform substructure. The method is verified further by nonlinear time history analysis methods for the regular 4-span bridge.

Current Analysis Methods of Seismically Isolated Bridges

Time History Analysis Methods

Time history analysis methods use nonlinear or equivalent linear properties for isolators and are suitable for complex structures when linear spectral methods are inappropriate or explicit modeling of the isolators and energy dissipaters is

required to better represent isolation systems that have high levels of damping. For the latter case, nonlinear time history analysis (NLTHA) is generally used. However, these methods require more computational time and largely depend on the ground motion record selection and scaling procedure to match the target spectrum.

Multimode Spectral Analysis Methods

When the Multimode Spectral Analysis (MMSA) is applied to an isolated bridge, an estimate of the design displacement must be made to determine the equivalent linear properties of the isolators. This is followed by iterations if the initial estimate has significant error. The 5 percent damped design spectrum is modified to recognize large amount of damping in the "isolated" modes. This is performed by scaling the spectrum by the damping reduction coefficient, B, for periods longer than 0.8 T_{eff}, where T_{eff} is the effective isolation period, which is calculated by the equivalent linear stiffness and damping properties of the isolators. The 5 percent damped spectrum is used for all other modes in the multimode method.

Current Simplified Methods

Both THA and MMSA account for the dynamic response of the entire bridge structure, including all components of the superstructure, isolation system, and substructure. In simplified methods, the superstructure is assumed to have a single degree of freedom corresponding to the horizontal displacement, the substructure and isolation system are reduced to a single spring having effective linear stiffness and equivalent damping properties. Figure 1 illustrates different models that have been proposed to perform simplified analysis for seismically isolated bridges.

Model A (isolated superstructure only): In this model, the superstructure is modeled as a single-degree-of-freedom (SDOF) system with mass M_{ss} and the piers are assumed infinitely rigid and massless. Thus, all the isolators supporting the superstructure experience the same displacement. The properties of individual isolators are lumped into a single isolator represented by its effective stiffness K_{iso}. Equivalent damping properties are used to reflect the energy dissipation capacity of the isolation system. The analysis requires iterations as stiffness and damping properties of the nonlinear isolators depend on the structure displacement. The flexibility and mass of the piers are totally ignored in this model (FHWA 2014).

Model B (flexible massless piers): Model B improves Model A by taking into account the horizontal stiffness of the piers in the bridge. At every pier, an effective stiffness is determined using the isolator effective stiffness K_{iso} and the pier stiffness K_p acting in series, and the total effective stiffness of the SDOF system is obtained by summing the effective stiffnesses of the individual piers. Equivalent damping representing energy dissipation of all isolators is also considered. Once the superstructure displacement is known, displacements and forces in each isolator and pier are determined based on

their respective stiffness properties. Likewise, the pier masses are not considered. This model has been adopted in North American codes such as AASHTO (2014) and CAN/CSA S6-14 (2014).

Model C (flexible piers with lumped 1/3 piers mass at the superstructure level): The masses of piers are taken into consideration by adding one-third of their masses to the superstructure. This transfer of mass increases the period of the system in an unrealistic way, which affects the demand on the isolation system, and the pier shear forces can have substantial errors (Priestley et al. 1996; Cardone et al. 2009; Buckle et al. 2011; Wei and Buckle 2012).

Model D (two SDOF systems with lumped 1/3 pier mass at the tops of piers): In this recently proposed model, the pier-isolator-superstructure unit is divided into two SDOF systems. One SDOF system considers only the superstructure mass and the other SDOF considers only the participating mass of the piers, which is assumed to be one-third of the pier masses. The effective stiffnesses of the isolators and piers are assumed equal in the two SDOF systems. The superstructure does not move in the second SDOF system. The results are obtained by combining the superstructure and pier results using the SRSS method (Wei et al. 2013; Al-Ani and Singh 2014).

In seismic isolated bridges, the substructure is not isolated from ground motions but merely decoupled from the relatively larger mass of the superstructure. Therefore, the pier base shears and moments contributed by the substructure mass are also important design parameters, in addition to the superstructure displacement. In the above four simplified models, the assumptions of rigid or massless piers or combining the pier mass equal to 1/3 (or a certain percentage) of the total pier mass are valid for bridges with light piers; however, they may lead to serious underestimation of the total base shears and moments in massive piers.

Proposed Simplified Method

Description and Assumptions

Figure 2 shows two new simplified models that are proposed to effectively consider the contributions of the pier masses to base shears and moments in the substructure.

Model E (superstructure SDOF system and flexible piers with mass): The whole bridge is modeled with two components: (1) the superstructure mass supported by the isolators and flexible massless piers acting in series at each pier, as in Model B in Fig. 1(b), and (2) flexible piers with distributed mass along their heights. Analysis of the first component permits to obtain the structure displacement, the displacements and forces in the isolators, and pier forces induced by the isolators. The second component is used to determine forces in the piers induced by their seismic responses. While the

analysis of the first component is iterative, as described earlier, analysis of the second component is not. The structural responses are obtained by the SRSS of the component results (Leroux 2015). In this model, the piers are free at their top ends in the second component, assuming that the piers are sufficiently stiff compared to the isolators such that their seismic responses are not significantly influenced by the response of the superstructure and isolators.

Model F (superstructure SDOF system and flexible piers with mass and top isolators): Model F is identical to Model E except that the effective stiffness of the isolators is introduced at the top of the piers in the second component. Parameters $k_{iso,i}$ and $k_{p,i}$ are effective stiffnesses of individual isolator and pier. Parameters K_{iso} ($K_{iso}=\Sigma k_{iso,i}$) and K_p ($K_p=\Sigma k_{p,i}$) represent the total effective lateral stiffnesses of the isolators and piers, respectively. The ratio of the total effective stiffnesses of the isolators to that of the piers varies depending on the simplified model used. The dynamic responses of the piers, including vibration periods and forces, are therefore influenced by the lateral restraint imposed by the isolators. After the analysis of the superstructure (first model component) is completed, individual piers are analyzed linearly using the isolators effective stiffnesses obtained from the superstructure analysis. Iterations are therefore not needed for the analysis of the piers. The final results are obtained by combining the results of the components using SRSS.

Analysis Methodology for Proposed Models E and F

For Models E and F, the analysis of the superstructure with isolators and massless piers (first model component) is performed using an equivalent SDOF system and an iterative approach, as currently specified in AASHTO and CAN/CSA S6-14 codes. A value is initially assigned to the superstructure displacement D_{ss}. The effective linear stiffnesses of the isolators are determined from this displacement, which allows for the calculation of the system effective stiffness and equivalent damping properties. Using these values, a new displacement is obtained from the design spectrum and the process is repeated until convergence is reached. Forces in each pier are obtained using their individual effective stiffnesses. The method is summarized herein for a bridge isolated with isolators exhibiting bilinear load-deformation response defined by the initial elastic stiffness k_e, the characteristic strength, Q_d, and the post-yield stiffness k_d, as will be used in the examples presented later. For this structure, the displacement in the isolator at pier i is obtained from:

$$D_{iso,i} = \frac{k_{p,i} D_{ss} - Q_{d,i}}{k_{d,i} + k_{p,i}} \tag{1}$$

where $k_{p,i}$ is the lateral stiffness of the pier. The force and effective stiffness of the isolator can then be determined:

$$F_{iso,i} = Q_{d,i} + k_{d,i} D_{iso,i} \tag{2}$$

$$k_{iso,i} = \frac{F_{iso,i}}{D_{iso,i}} \tag{3}$$

The effective stiffness of each pier $k_{eff,i}$ is the combined stiffness of the pier and the isolator acting in series:

$$k_{eff,i} = \frac{k_{iso,i} \times k_{p,i}}{k_{iso,i} + k_{p,i}} \tag{4}$$

The effective period of the SDOF system, T_{eff} , is then given by:

$$T_{eff} = 2\pi \sqrt{\frac{M_{ss}}{K_{eff}}} \tag{5}$$

where M_{ss} is the superstructure mass and K_{eff} is the total effective lateral system of the SDOF system: $K_{eff} = \sum k_{eff,i}$.

The new superstructure displacement, D_{ss} , is computed from:

$$D_{ss} = \frac{S_d(T_{eff})}{B} \quad \text{, where } B = \left(\frac{\xi}{0.05}\right)^{0.3} \tag{6}$$

In this equation, $S_d(T_{eff})$ is the 5% damped displacement spectral value for the site at the period T_{eff}, B is the damping reduction coefficient and ξ is the equivalent damping ratio for the bridge-isolator system. The latter is obtained from the total energy dissipated per cycle by all isolators, *EDC*, when the structure oscillates at the displacement D_{ss}:

$$\xi = \frac{EDC}{2\pi K_{eff} D_{ss}^2} \tag{7}$$

The new displacement D_{ss} is used in subsequent iterations until convergence is achieved. Forces $F_{p,i}$ at the top of each pier are then computed to determine shears and bending moments in the piers due to the superstructure displacement:

$$F_{p,i} = k_{eff,i} D_{ss} \tag{8}$$

Analysis of the second component of Models E and F is performed to obtain the additional shears and bending moments in the piers due to the dynamic seismic response of the piers themselves. Elastic models of the piers are established using the actual mass and stiffness distribution of each pier. For Model F, the effective stiffness of each isolator $k_{iso,i}$ is taken equal to the value obtained in the last iteration of the superstructure analysis. Using the 5% damped acceleration spectrum at the site, the individual piers are elastically analyzed using the modal response spectrum method, from which the internal forces of individual piers can be obtained. Forces in the isolated bridge are then obtained by combining the results of the superstructure and piers using the SRSS method.

Typically, the seismic demand on individual piers can be obtained from their first mode response. For a single pier with uniform stiffness and mass properties, the fundamental period is given by Eq. (9). For Model E, λ_1 = 1.875. For Model F, λ_1 is the minimum positive root of the frequency equation given by Eqs. (10) and (11) (Karnovsky and Lebed 2000):

$$T_1 = 2\pi/\omega_1 = 2\pi \Big/ \left(\frac{\lambda_1^{\,2}}{H^2} \sqrt{\frac{E_c I_{cr}}{m}} \right) \tag{9}$$

$$\lambda^3 \frac{1+\cos\lambda\cosh\lambda}{\sinh\lambda\cos\lambda - \sin\lambda\cosh\lambda} = k \tag{10}$$

$$k = \frac{k_{iso,i} H^3}{E_c I_{cr}} \tag{11}$$

where m is the pier mass per unit length, H is the pier height, E_c is the modulus of elasticity, I_{cr} is the effective inertia moment of the pier in the vibration direction, and $k_{iso,i}$ is the effective stiffness of the isolator. Alternatively, using the value of k from Eq. (10), λ_1 can be determined from Fig. 3.

The first mode shape ϕ_1(x) is computed as follows.

$$\phi_1(x) = \sinh\lambda_1 \frac{x}{H} - \sin\lambda_1 \frac{x}{H} - \frac{\sin\lambda_1 + \sinh\lambda_1}{\cos\lambda_1 + \cosh\lambda_1} (\cosh\lambda_1 \frac{x}{H} - \cos\lambda_1 \frac{x}{H}) \tag{12}$$

where x is the distance from the pier base. Thus, the fundamental period and mode shape of the pier with uniform mass and stiffness can easily be computed, and the analysis of the pier component is simple. Later in the paper, accuracy of using single mode pier response is verified against the solution obtained with the MMSA method. For more complex pier geometries, multimode pier response can be computed using a structural analysis program.

Range of Validity for Different Simplified Methods for a Regular Bridge Structure

Bridge Model and Seismic Input

The bridge selected in this study is representative of regular multi-span highway bridges with continuous superstructure, prestressed concrete box girders with symmetrical geometry and four piers of equal height. The geometry and dimensions of the piers and superstructure are illustrated in Fig. 4. The piers have uniform rectangular cross-sections with a width of 12.6 m. The piers at intermediate supports are however thicker (4 m) compared to those at the bridge ends (3.2 m). The girder depth varies from 9.5 m at the intermediate supports to 3.5 m at the midspan as a parabolic curve. The mass properties of the

superstructure and separate components are given in Table 1. For this bridge, the M_p/M_{ss} ratio is 0.40. With such a high mass ratio, the bridge would classify as a bridge with "massive piers" (Buckle et al. 2011; Wei et al. 2013; Al-Ani and Singh 2014). Table 1 also gives the lateral stiffness properties of the piers, $k_{p,i}$. Herein, a reduced flexural stiffness is taken equal to 0.7 E_cI_g , where I_g is the moment of inertia of the gross, uncracked cross-section, as recommended for reinforced concrete members when only a moderate amount of cracking and no plastic hinging is expected (ATC 1996). As shown, pier 2 is 25% more massive and approximately twice as stiff as pier 1. A more rigorous approach to define the cracked flexural stiffness, EI_{cr}, is to perform a nonlinear moment-curvature reinforced concrete cross-section analysis to compute the cracking moment, M_{cr}, and identify EI_{cr}. However, nonlinear cross-section analysis is deemed unnecessary while using the proposed simplified analysis method in preliminary design.

The bridge is isolated at every pier for the seismic demand along the longitudinal direction and the Friction Pendulum System (FPS) is selected for the seismic isolators. The force-displacement hysteresis loop for FPS isolators is shown in Fig. 5. The characteristic strength of the isolator is the force at initiation of slip (D_{iso} = 0), i.e, $Q_d = \mu W$, whereas the post-yield stiffness, k_d, is equal to W/R. The initial stiffness k_e is assumed infinite. The horizontal force F_{iso}, at any displacement D_{iso} can then be obtained from (Earthquake 1999; Dicleli and Mansour 2003):

$$F_{iso} = \mu W + \frac{W}{R} D_{iso} \tag{13}$$

In the SM and MMSA analyses, the effective isolator stiffness k_{iso} is used and the equivalent viscous damping ratio of the system, ξ , is obtained to reflect the energy dissipation of the isolators. The effective stiffness of the isolator is obtained by dividing the maximum horizontal force by the maximum isolator displacement, D_{iso}.

$$k_{iso} = \frac{\mu W}{D_{iso}} + \frac{W}{R} \tag{14}$$

For FPS isolators, the energy dissipated per cycle corresponds to the area enclosed by the hysteresis loop: $EDC = 4\ \mu W\ D_{iso}$. The total value of EDC for the bridge is used in Eq. 7 to determine ξ of the equivalent linear system.

The radius R and friction coefficient μ of the isolators at all piers are chosen as 4 m and 0.03 respectively, and the main parameters for the isolators are given in Table 1. As shown, the resistance and post-yield stiffness of the isolators at the interior piers are much larger than at the exterior piers due to the differences in vertical reactions between the two piers.

The bridge is assumed to be located on a class C site in Vancouver, British Columbia, and the design of the isolation system is performed in accordance with CAN/CSA S6-14. In CAN/CSA S6-14, the design seismic input is represented by the

5% damped uniform hazard acceleration response spectrum (UHS) established for a probability of 2% in 50 years. The acceleration spectrum and corresponding displacement spectrum are plotted in Fig. 6. The peak ground acceleration for this site and same hazard level is PGA=0.369 g.

When the bridge is analyzed with Simplified Methods using Models A to F, the displacement spectrum shown in Fig. 6(b) is used to determine the bridge displacement. The 5% damped response spectrum of Fig. 6(a) is used for the analysis of the second component of Models E and F. When a MMSA is conducted, the 5% damped acceleration spectrum (Fig. 6a) is used except that it is modified for larger damping in the fundamental mode of vibration introduced by the isolators. This modification is performed by dividing all spectral acceleration values at periods longer than 0.8 times the effective period of the bridge, T_{eff}, by the damping reduction factor, B obtained with the equivalent viscous damping ratio ξ from Eq. (7).

Simplified Methods versus Multimodal Spectral Analysis

For Model A, the effective stiffness at each pier is taken equal to the effective stiffness of the isolator at that pier. For Model B, the effective stiffness of the bridge system is derived by combining the isolator and pier stiffnesses in series. For Model C, the superstructure mass is increased by 1/3 of the pier masses compared to the method used in Model B. For Models D, E, and F, the first component is the same as that used in Model B. In the second component of Models D and F, the effective stiffness of the isolators is equal to that obtained in the first component and only the first mode response of the piers is considered. The main difference between Models D and F is that Model D lumps 1/3 of all pier masses on the top of the pier, whereas Model F uses the actual pier mass distribution. Table 2 gives the results obtained from Models A to F. Detail of the calculations for Models E and F is given in Appendix I.

When MMSA is used, the analysis of the bridge is conducted with a 3D MDOF model of the bridge using the finite-element structural analysis software SAP2000 (CSI 2014). The superstructure is modeled using 3D beam elements, which are divided into a number of segments, and its mass is lumped at each nodal point connecting the segments. The superstructure mass is assigned only to the horizontal degree of freedom of the nodes to avoid triggering insignificant modes of vibration that are not useful in the analysis because only the seismic response in the longitudinal direction is considered in this study. Each pier is also modeled with beam elements, and their tributary masses are lumped at the nodes connecting each segment. Likewise, for each pier node, the pier mass is assigned only to the horizontal degree of freedom. In the MMSA, effective linear springs and equivalent viscous damping are used to represent the isolators. The model is iteratively analyzed to obtain final estimates of the superstructure displacement and the required effective properties of each isolator. The results from the

simplified Model A are used to determine the initial values for the effective damping and stiffness of the isolators to initiate the iterative process. Table 2 also gives the results of the MMSA, which are used as the reference solutions.

Figure 7 illustrates the comparisons of the isolated periods, superstructure displacements, and shear forces and bending moments at pier bases from all models. The SM results are all normalized by the MMSA results. Due to symmetry, only the forces in piers 1 and 2 are plotted.

According to Table 2 and Fig. 7, there are no significant differences regarding periods and displacements among the various models, except for Model C which overestimates the isolated period and superstructure displacement. Conversely, the accuracies of the pier base shears and moments vary dramatically for different models. Models E and F provide very accurate results for both piers. Models A to C significantly underestimate the shears and moments at pier bases, especially for pier 1 for which the minimal ratio with the MMSA is approximately 0.1. Although Model D gives better approximations compared to those of models A-C, it still exhibits large discrepancies compared to the MMSA. Therefore, for this particular bridge structure, Models E and F are capable of yielding accurate results for predicting the reference values from the MMSA.

For this bridge with massive piers, the ratio of the total effective stiffnesses of the isolators ($K_{\mathrm{iso}} = \Sigma k_{iso,i}$) to that of the piers ($K_{\mathrm{p}} = \Sigma k_{p,i}$) varies between 0.0273 to 0.0279 depending on the model used. This small ratio indicates that the piers are relatively very stiff and the isolators at the top of the piers do not affect much the dynamic response of the individual piers (piers can vibrate under the superstructure as independent structures). This is why Models E and F give almost equal results. However, this is not always valid. When the piers are not so stiff, differences exist, and omitting the isolator stiffness at the pier tops in Model E may decrease the accuracy of this model, as will be shown in the next section.

Influence of Bridge Stiffness and Mass Properties on the Accuracy of Simplified Methods

To assess and compare the accuracy of the different simplified models A to F under a number of mass ratios and stiffness ratios, SMs and MMSAs were performed on the same bridge structure with M_p/M_{ss} ratios ranging from 0.05 to 0.60 and K_{iso}/K_p ratios ranging from 0.03 to 0.36. These ratios were obtained by changing the pier masses and pier stiffnesses independently. In the process, the relative mass and stiffness properties between piers 1 and 2 were preserved and the properties of the isolators remained unchanged. The ranges of mass and stiffness ratios were selected to be reasonable for seismically isolated bridges (Wei et al. 2013; Al-Ani and Singh 2014). The results of this comprehensive parametric analysis were used to identify the ratios at which the assumptions of rigid or massless piers or lumping the pier masses equal to 1/3rd of the total pier masses cause significant unconservatism. The acceptance criterion for a simplified method of seismically isolated bridges is typically limited to within 0.9-1.1 of the reference MMSA values.

Figure 8 compares the seismic responses from Model A to the results from MMSA for the different mass and stiffness ratios. For all mass ratios, superstructure displacements D_{ss} and effective periods T_{eff} from Model A can provide good estimates of superstructure displacements and first-mode periods T_1 when $K_{iso}/K_p \leqslant 0.15$. When the pier is more flexible compared to the isolation system, both the displacements and effective periods are underestimated using Model A. In Figs. 8c and 8e, for all mass and stiffness ratios, Model A considerably underestimates the base shears and moments at the more flexible pier 1. The situation is less critical for the stiffer and more massive pier 2 as Model A predicts reasonable and even conservative force demands for small mass ratios and high stiffness ratios. For this pier, shears are however underestimated when $M_p/M_{ss} > 0.15$ to 0.24 and moments are underestimated when $M_p/M_{ss} > 0.2$ to 0.5. For both piers, the errors are also less pronounced for bending moments compared to shears. Nevertheless, Model A is therefore not appropriate for designing bridges with massive piers.

Figure 9 compares the seismic responses from Model B to those from MMSA. This model can better predict the superstructure displacements and first periods because pier flexibility is taken into account in the calculations. For all mass ratios and stiffness ratios, the accuracies of displacements and first periods are within the acceptance range of 0.9-1.1. However, similar to Model A, Model B significantly underestimates the shears and moments in pier 1 and generally give non-conservative force estimates for pier 2, except for small mass ratios, less than approximately 0.15 for shears and 0.20 for moments. Exact limits also depend on the stiffness ratio. Model B is still not appropriate for designing bridges with massive piers.

The seismic responses from Model C is examined in Fig. 10. This model consistently overestimates the superstructure displacements and first mode periods for all stiffness ratios and mass ratios. The errors increase as the mass ratio is increased or the stiffness ratio is decreased. Like Model B, the pier shear forces and moments are substantially underestimated for larger stiffness and mass ratios. For the base shears in pier 2, the mass ratios (M_p/M_{ss}) must still be limited to within 0.15 to meet the acceptance criteria for all stiffness ratios. That limit can be extended to 0.2 for bending moments.

Figure 11 presents the base shears and moments from Model D. For this model, the superstructure displacements and first periods are similar to those from Model B. As shown in the figure, Model D yield better predictions of shears and bending moments in both piers. For pier 1, however, both the base shears and bending moments are still underestimated for all stiffness and mass ratios. In pier 2, acceptable shears and moment estimates are obtained when $M_p/M_{ss} \leqslant 0.20$ and $M_p/M_{ss} \leqslant 0.50$, respectively, regardless of the stiffness ratio.

The seismic responses from Model E are given in Fig. 12. In Models E and F, the first component of the model corresponds to Model B and the structure displacements and effective periods are therefore same and correspond well to the MMSA predictions shown in Fig. 9. These comparisons are not repeated here. In Figs. 12 (a) and (b), the fundamental periods of the individual piers in the model second component, T_{p1} and T_{p2}, are compared to the periods corresponding to the fundamental modes of these piers in the 3D structure model (T_2 and T_3). As shown, periods T_{p1} and T_{p2} are longer than their 3D model counterparts because the stiffness of the isolators is not included at the top of the piers in the model second component. Overall, Model E gives relatively accurate estimates of the forces acting in the piers. As shown, shears and moments are generally on the conservative side and generally less than 1.10 times the values obtained from MMSA. Values in excess of this limit are obtained for the structures with larger K_{iso}/K_p values.

The results from proposed Model F are compared to those from MMSA in Figure 13. For this model, the periods of the individual piers match very well those obtained from the structure 3D model because isolator stiffness is considered at the top end of the piers. The model also gives very accurate predictions of the base shears and moments as the ratios for all seismic forces are within the 0.9-1.1 range for all the stiffness ratios and mass ratios considered in the study. When compared to Model E, improvements in predictions are attributed to the better representation of the boundary conditions for the individual piers in the model second component. Thus, Model F can be safely used for both initial and final designs of regular seismically isolated bridges with $K_{iso}/K_p \leq 0.36$ and $M_p/M_{ss} \leq 0.60$.

Generalization Considering an Irregular Bridge Structure with Different Pier Heights

In this section, a bridge with non-prismatic massive piers having different heights is selected to verify the accuracy of the proposed models E and F. As in the previous example, the bridge is assumed to be located on a site class C in Vancouver, BC, and its seismic response is examined in the longitudinal direction. For such a bridge with complex pier geometries, analytical solutions of the dynamic characteristics of the piers are not available. The stiffness properties of the piers ($k_{p,i}$) for the model first component and the seismic force demands on individual piers for the model second component are therefore obtained from finite element (FE) analysis of the piers. As the analysis of the individual piers is linearly elastic and no additional iteration is required, using the simplified method with Models E and F is still much simpler than MMSA.

Description of the Bridge

The geometry of the multi-span continuous girder bridge considered in this section is given in Fig. 14. The bridge has five 50 m spans with a superstructure composed of a multi-cellular steel girder supported on four intermediate V-shaped

concrete piers and two abutments at the ends. The bridge is symmetrical with respect to its mid-length. As shown, piers 1 and 4 are 12 m high whereas piers 2 and 3 are 16 m high. The elevation of the 16 m tall piers is illustrated in the figure. The total weight of the superstructure is W=79547 kN, with moments of inertia about the strong and weak axes of I_y=87.57 m^4 and I_x=1.37 m^4, respectively, and a modulus of elasticity of E=200 GPa. As in the previous example, the flexural stiffness of the pier was obtained using 70% of the gross section stiffness of the piers to account for concrete cracking. In the longitudinal direction, the lateral stiffnesses of individual piers 1 and 2 are 415973 kN/m and 208030 kN/m, respectively. The two abutments are assumed to be infinitely stiff. The total mass of the piers and abutments is 0.32 times the mass of the superstructure.

The seismic isolators at each pier and abutment are composed of two identical High Damping Rubbers (HDR) which are assumed to exhibit a bilinear hysteretic force-displacement curve as shown in Fig. 15. For this example, the total values of parameters k_e, Q_d, and k_d, for the two isolators at each support are 71451 kN/m, 1377 kN, and 5880 kN/m, respectively.

The 3D finite element model used in MMSA and NLTHA is shown in Fig. 16. The superstructure and piers are expected to remain within the linear elastic range and were modeled as linear elastic beam-column elements. As for nonlinear isolators, link elements are selected to represent the effective linear stiffnesses in MMSA. In NLTHA, links exhibiting bi-linear responses were used. Modeling of the piers in Models B, E and F was identical as was used in the 3D bridge model.

Comparisons of Results from Model B, Proposed Models E and F and MMSA

The purpose of this paper is to extend the range of application of simplified models currently used in relation to AASHTO and CAN/CSA S6-14. Model B has been most often adopted when a simplified design method is used. Our previous results from a regular highway bridge show that Models A, C and D are not appropriate for designing bridges with massive piers. However, Models E and F are able to improve significantly result accuracy as compared to Model B. Therefore, to further confirm the applicability of the proposed models (E, F) in a bridge with complex piers, only results from Models B, E, and F are compared in this section of the paper. At the end of the iterative procedure with Model B, $k_{iso,1}$ = 16797 kN/m, $k_{iso,2}$ = 17243 kN/m, T_{eff} = 1.82 s, ξ = 33%, and the superstructure displacement is 0.131 m. With these values, the stiffness ratio for the bridge considering only piers 1 to 4 is 0.08. The results obtained from Model B and proposed Models E and F are compared with the reference results from the MMSA in Table 3. As for the previous bridge structure, Model B provides a good estimate of the structure displacement and effective period but under-predicts shears and bending moments at the bases of the piers. Conversely, Models E and F give displacement, period and pier force estimates that are in the range of 1.02-1.08 and 1.00-1.08, respectively. For such a bridge, with different pier heights and complex pier geometry,

the simplified method using proposed Models E and F can therefore provide good accuracy and simplicity compared to the relatively complex MMSA.

Comparisons of Results from Simplified Methods and NLTHA

In the preceding sections, the responses from the simplified methods have been compared with the results of MMSA. While MMSA can account for the contribution of higher vibration modes, there are some approximations in this method, such as (1) the equivalent linearization of isolators and (2) modal combination methods (SRSS, CQC). To better assess the validity of Models E and F, the results from these methods are compared to those obtained from nonlinear time history analysis (NLTHA) for the regular 4-span bridge studied earlier. A horizontal ground motion accelerogram recorded at the Coyote Lake Dam station during the 1989 Mw 6.93 Loma Prieta earthquake is used. This acceleration time history and corresponding response spectrum are illustrated in Fig. 17. As shown, this record was selected because it matches well the design spectrum in the period range of interest. Nevertheless, in order to eliminate differences between spectral based analysis methods and NLTHA due to dissimilarities between spectral shapes and effects of ground motion scaling, the simplified analysis with Model F and the MMSA were performed using the ground motion spectrum rather than the design spectrum.

Numerical integration in NLTHA was performed using the Newmark-Beta approach with a constant time step of 0.005 s. Rayleigh damping corresponding to 5% of critical in the mode associated with was considered. As explained in the CSI Analysis reference manual (CSI 2014), the damping matrix for element j is computed as follows:

$$C_j = c_m M_j + c_k K_j \tag{15}$$

where c_m and c_k are the mass and initial (elastic) stiffness-proportional damping coefficients, M_j is the mass matrix and K_j is the initial stiffness matrix. During the NLTHA, problems associated with inaccurate damping forces and the inelastic softening of nonlinear isolators are solved by transferring stiffness-proportional damping from the dynamic load case, for the entire structure, to the materials of individual components. This is performed as follows: (1) in the time-history load case, the c_m value is kept, but c_k becomes zero; and (2) for all elastic materials (superstructure and piers), c_k is set to the initial elastic value. The energy dissipation of seismic isolators is then considered only based on its nonlinear force-displacement hysteretic actions.

The seismic responses from the simplified method with Model F and from MMSA are compared with the reference results from the NLTHA in Table 4. The results from Model F and MMSA are different from those given in Table 2 because

the analyses were performed using the ground motion spectrum. As was observed when using the design spectrum, both methods here give very similar results. As discussed previously, Model F and MMSA give very similar results. When compared to NLTHA, Models F and MMSA over-predict the superstructure displacement by approximately 20%. However, both approaches predict pier base shears and moments that are within 0.90-1.15 times the results from NLTHA. The maximum errors are for the base shear in pier 2 which is also over-estimated by a greater margin (15% for Model F and 13% for MMSA). These differences are mainly due to the simplification made when using an equivalent linear system is used in spectral based method to predict the response of a structure that includes a nonlinear isolation system. Hence, for this particular bridge, the simplified method with Model F yields satisfactory approximations compared to the rigorous NLTHA method.

Conclusions

Two enhanced models are proposed and validated for the application of the simplified method specified in North American codes for the seismic analysis of isolated highway bridge structures with massive substructures. In the first model, "Model E", the bridge is divided into two independent components: a first component which is an equivalent SDOF system that includes the superstructure, the isolators, and the flexible massless piers, and the second component which includes the flexible massed piers. "Model F" is identical to Model E except that the stiffness of the isolators is added at the top of the piers in the second component. In both models, the first component corresponds to the model already described in the 2014 AASHTO and CAN/CSA S6-14 standards for the simplified analysis method. Seismic analysis results from both components are combined using the SRSS method. The applicability of the two models was verified for regular and irregular bridges having ratios of the masses of piers to the mass of the superstructure, M_p/M_{ss}, between 0.05 and 0.6 and ratios between the isolators stiffness and piers stiffnesses, K_{iso}/K_p, varying between 0.03 to 0.36. Results from the two models were compared to those obtained from multimode spectral and nonlinear time history analyses. The following conclusions can be drawn from this study:

The simplified analysis methods using currently available Models A to D generally give good estimates of the superstructure displacements and first-mode effective periods. However, for most of the bridges analyzed, they underestimate the shear and moment demands at the pier bases, with the errors being more important when the mass ratio M_p/M_{ss} is increased and the stiffness ratio K_{iso}/K_p is decreased.

Proposed Models E and F both yield improved shear and moment predictions for the separate components. For the bridges studied, Model E gives predictions higher than 0.9 times the results from multimode spectral analysis but can result

in overly conservative force demands for bridges with larger stiffness ratios. This excessive conservatism is mitigated when using Model F. In addition, Model F is found to give satisfactory predictions of pier base shears and moments compared to those from rigorous nonlinear time history analysis. In view of the small added computational complexity of Model F compared to Model E, Model F is thus recommended to achieve safe and cost-effective solutions.

Acknowledgements

This research was supported by the Key Consulting Project of Chinese Academy of Engineering (Grant no. 2016-XZ-13). The authors would like to acknowledge financial support from the China Scholarship Council (CSC) and the Natural Sciences and Engineering Research Council of Canada (NSERC).

References

AASHTO. (2014). *Guide specifications for seismic isolation design*, 4th Edition, Washington, D.C., USA.

Adhikari, G., Petrini, L., and Calvi, G.M. (2010). "Application of direct displacement based design to long span bridges." *Bulletin of Earthquake Engineering*, (8): 897-919.

Al-Ani, M., and Singh, C. (2014). "Influence of substructure properties on analysis and design of seismically-isolated bridges." *Proc., 9th Austroads Bridge Conf.*, Sydney, New South Wales, Australia.

Applied Technology Council (ATC). (1996). *Seismic Evaluation and Retrofit of Concrete Buildings*, Redwood City, Calif., USA.

Buckle, I.G., Al-Ani, M., and Monzon, E. (2011). *Seismic isolation design examples for highway bridges*. Technical Rep. No. NCHRP Project 20-7-Task 262, National Cooperative Highway Research Program, Washington, D.C., USA.

Buckle, I.G., Constantinou, M., Dicleli, M. and Ghasemi, H. (2006). *Seismic isolation of highway bridges*. Technical Rep. No. MCEER-06-SP07, State Univ. of New York at Buffalo, Buffalo, N. Y., USA.

Cardone, D., Dolce, M., and Palermoa, G. (2009). "Evaluation of simplified methods for the design of bridges with seismic isolation systems." *Earthquake Spectra*, 25(2), 221-238.

Constantinou M. C., Kalpakidis I., Filiatrault A., and Ecker Lay R.A. (2011). *LRFD-Based analysis and design procedures for bridge bearings and seismic isolators*. Technical Rep. No. MCEER-11-0004, State Univ. of New York at Buffalo, Buffalo, N. Y., USA.

CSA (2014). "Canadian highway bridge design code", *CAN/CSA-S6-14*, *Canadian Standards Association (CSA*), Rexdale, Toronto, Canada.

CSI (2014). *SAP2000: Integrated finite element analysis and design of structures basic analysis reference manual*. Computers and Structures Inc., Berkeley CA., USA.

Dicleli, M., and Mansour, M. (2003). "Seismic retrofitting of highway bridges in Illinois using friction pendulum seismic isolation bearings and modeling procedures." *Eng. Struct.*, 25(9):1139-1156.

Dicleli, M., Mansour, M. Y., and Constantinou, M. C. (2005). "Efficiency of seismic isolation for seismic retrofitting of heavy substructured bridges." ASCE *J. Bridge Eng.*, 10(4), 429-441.

Earthquake Protection Systems Inc. (1999). *Friction pendulum seismic isolation bearing: Details and specifications for bridges*. Richmond, Calif., USA.

Fadi, F., and Constantinou, M. C. (2010). "Evaluation of simplified methods of analysis for structures with triple friction pendulum isolators." *Earthquake Engng Strut. Dyn.*, 39(1), 5-22.

Federal Highway Administration (FHWA). (2014). LRFD seismic analysis and design of bridges reference manual. Publication No. FHWA-NHI-15-004, U.S. Dept. of Transportation, Washington, D.C., USA.

Feng, M. Q., and Lee, S. C. (2009). *Determining the effective system damping of highway bridges.* Rep. No. CA-UCI-2009-00, Univ. of California, Irvine, Calif., USA.

Franchin, P., Monti, G., and Pinto P. E. (2001). "On the accuracy of simplified methods for the analysis of isolated bridges." *Earthquake Engng Strut. Dyn.*, 30: 363-382.

Guyader, A. C., and Iwan, W. D. (2006). "Determining equivalent linear parameters for use in a capacity spectrum method of analysis." ASCE *J. Struct. Eng.*, 132(1), 59-67.

Hwang, J.S., Chang, K.C., and Tsai, M.H. (1997). "Composite damping ratio of seismically isolated regular bridges." *Eng Struct*, 19(1), 55-62.

Jara, M., and Casas, J. R. (2006). "A direct displacement-based method for the seismic design of bridges on bi-linear isolation devices." *Eng Struct*, 28(6), 869-879.

Jara, M., Jara, J. M., Olmos, B. A., and Casas, J. R. (2012). "Improved procedure for equivalent linearization of bridges supported on hysteretic isolators." *Eng Struct*, 35, 99-106.

Karnovsky, I.A., and Lebed, O.I. (2000). Formulas for Structural Dynamics: Tables, Graphs and Solutions.. McGraw Hill Inc. New York, USA.

Leroux, M. (2015). *Seismic isolation: A study of inertial forces in bridge's piers.* Master of Engineering thesis, Ecole Polytechnique de Montreal, Quebec, Canada (in French).

Ozdemir, G., and Constantinou, M. C. (2010). "Evaluation of equivalent lateral force procedure in estimating seismic isolator displacements." *Soil Dyn. Earthquake Eng.*, 30(10), 1036-1042.

Priestley, M. J. N., Seible, F., and Calvi, G. M. (1996). *Seismic design and retrofit of bridges*. Wiley, New York, USA.

Reinhorn, A. M., Simeonov, V. K., DeRue, G., and Constantinou, M. C. (1998). *Sensitivity of response of isolated bridges to modeling and design parameters: A case study*. Technical Rep. No. 98-0015, Columbia Univ., New York, USA, 213-223.

Tsopelas, P., Constantinou, M. C., Kircher, C. A., and Whittaker, A. S. (1997). *Evaluation of simplified methods of analysis for yielding structures*. Technical Rep. No. NCEER-97-0012, State Univ. of New York at Buffalo, Buffalo, N. Y., USA.

Wei, C., and Buckle, I.G. (2012). "A simplified method of analysis of isolated bridge with yielding substructure." *Proc. Structures Congress*, ASCE, Chicago, USA, 559-570.

Wei, C., Al-Ani, M., and Buckle, I.G. (2013). "An improved simplified method for the analysis of seismically isolated highway bridge with heavy substructure." *Proc., 7th National Seismic Conf. on Bridges and Highways*, Oakland, CA, USA, 1-7.

Appendix I. Manual calculation examples using Models E and F

This appendix provides detail of the calculations of the shear forces and moments at the base of pier 2 of the regular 4-span bridge in Fig. 4 using the simplified method with Models E and F. The final results of the calculations presented herein are summarized in Table 2, and the accuracy of Models E and F is verified against MMSA results in Fig. 7. Properties of the piers and Model B used for the superstructure analysis (model first component) are given first. For each model, analysis of individual pier 2 (model second component) is then described and the results are combined with those from Model B analysis.

Properties of the Piers

Piers heights: $H_1 = H_2 = 17.5$ m

Distributed mass of the piers: $m_{p,1} = 98.7$ tons/m; , $m_{p,2} = 123.4$ tons/m

Modulus of elasticity of concrete: $E_c = 3.25\text{x}10^7$ kPa

Moment of inertia of the gross section of the piers: $I_{g,1} = 34.4$ m^4; $I_{g,2} = 67.2$ m^4

Lateral stiffness of the piers:

pier 1: $0.7E_cI_{g,1} = 0.7\text{x}3.25\text{x}10^7\text{x}34.41 = 0.783\text{x}10^9$ kNm^2 => $k_{p,1} = 3\text{x}(0.783\text{x}10^9)/17.5^3 = 438200$ kN/m

pier 2: $0.7E_cI_{g,2} = 0.7\text{x}3.25\text{x}10^7\text{x}67.20 = 1.529\text{x}10^9$ kNm^2 => $k_{p,2} = 3\text{x}(1.529\text{x}10^9)/17.5^3 = 855800$ kN/m

Model B (first component of Models E and F)

In the final iteration, $D_{ss} = 0.235$ *m,* which gives:

$D_{iso,1}$ = (438200x0.235–338)/(2820+438200) = 0.233 m (Eq. 1)

$F_{iso,1} = F_{p,1} = V_{p,1}$ = 338+2820x0.233 = 995 kN (Eq. 2)

$M_{p,1}$ = 995x17.5 = 17413 kN.m

$k_{iso,1}$ = 995/0.233 = 4270 kN/m

$k_{eff,1}$ = (4270x438200)/(4270+438200) = 4229 kN/m (Eq. 4)

$D_{iso,2}$ = (855800x0.235 – 2500)/(20836+855800) = 0.2267 m (Eq. 1)

$F_{iso,2} = F_{p,2} = V_{p,2}$ = 2500 + 20836x0.2267 = 7223 kN (Eq. 2)

$M_{p,2}$ = 7223x17.5 = 126400 kN-m

$k_{iso,2}$ = 7223/0.2267 = 31867 kN/m

$k_{eff,2}$ = (31867x855800)/(31867+855800) = 30723 kN/m (Eq. 4)

$K_{eff,}$ = 2(4229+30723) = 69904 kN/m

$T_{eff} = 2\pi(19310/69904)^{0.5}$ = 3.302 s

$S_d(3.302\ s)$ = 0.362 m

EDC = 2(4x338x0.233 + 4x2500x0.2267) = 5164 kN.m

$\xi = 5164/(2\pi \text{ x}69904\text{x}0.235^2) = 21.3\%$

$B = (0.213/0.05)^{0.3} = 1.545$

new D_{ss} = 0.362 m / 1.545 = 0.234 m (close to assumed value)

Forces in pier 2 using Model E

First-mode vibration period

For Model E, the pier in the model second component vibrates like a cantilever as there is no translational spring support at the pier top. The first-mode period is obtained from Eq. (9) with the frequency parameter λ_1 = 1.875.

$$T_{p,2} = 2\pi \Bigg/ \left(\frac{1.875^2}{17.5^2} \sqrt{\frac{1.529 \times 10^9}{123.4}} \right) = 0.155\ s$$

The acceleration spectrum value (5% damping ratio) is obtained from Fig. 6a.

$$S(T_{P2}) = 0.848\ g$$

Mode shape and modal participation factor

The pier is divided into 20 elements, and the modal coordinates for each node are computed from Eq. (12) using a spreadsheet:

$$\{\phi_1\}^T = \{0.0030, 0.0260, 0.0705, 0.1349, 0.2174, 0.3165, 0.4306, 0.5580, 0.6972, 0.8468, 1.0051, 1.1709, 1.3429, 1.5197, 1.7004, 1.8839, 2.0692, 2.2558, 2.4430, 2.6305\}$$

The corresponding mass matrix and influence vector are as follows:

$$[M]_{(ton)} = diag\left(\begin{bmatrix} 108, 108, 108, 108, 108, 108, 108, 108, 108, 108, \\ 108, 108, 108, 108, 108, 108, 108, 108, 108, 108 \end{bmatrix}\right)$$

$$\{r\}^T = \{1,1,1,1,1,1,1,1,1,1,1,1,1,1,1,1,1,1,1,1\}$$

and the modal participation factor is obtained from:

$$\gamma_1 = \frac{\{\phi_1\}^T [M]\{r\}}{\{\phi_1\}^T [M]\{\phi_1\}} = 0.575$$

Pier shear and moment distribution

The nodal inertia forces along the pier heights are computed from the following relationship.

$$\{V_{P2}\}^T{}_{(kN)} = \gamma_1 S_a(T_{P2})[M]\{\phi_1\} = \{2, 13, 36, 70, 112, 163, 222, 288, 360, 437, 519, 605, 693, 785, 878, 973, 1068, 1165, 1261, 1358\}$$

The pier is then analyzed under these loads to obtain shears and bending moments along the pier heights shown in Fig. 18.

The pier base shear and moment from this second component analysis, as noted by the *"p"* superscript, are $V_{P2}{}^p = 11010\,kN$ and $M_{P2}{}^p = 139900\,kN.m$, respectively. According to Table 2, the base shear and moment of the superstructure (first component), as noted by the *"ss"* superscript, are $V_{P2}{}^{ss} = 7223\,kN$ and $M_{P2}{}^{ss} = 126400\,kN.m$, respectively. Then, the design base shear and moment for Model E shown in Table 2 (as noted by the *"E"* superscript) are computed using the SSRS method:

$$V_{P2}^E = \sqrt{(V_{P2}{}^{ss})^2 + (V_{P2}{}^p)^2} = \sqrt{7223^2 + 11010^2} = 13168\,kN \qquad \text{(see Table 2)}$$

$$M_{P2}^E = \sqrt{(M_{P2}{}^{ss})^2 + (M_{P2}{}^p)^2} = \sqrt{126400^2 + 139900^2} = 188544\,kN.m \qquad \text{(see Table 2)}$$

The design shear force and bending moment computed by MMSA (denoted using the *"MMSA"* superscript) are $V_{P2}^{MMSA} = 13350\,kN$ and $M_{P2}^{MMSA} = 185396\,kN.m$, respectively. Finally, the accuracies of the base shear and moment shown in Fig. 7 are:

$$V_{P2}^{E} / V_{P2}^{MMSA} = 13168 / 13350 = 0.99$$

$$M_{P2}^{E} / M_{P2}^{MMSA} = 188544 / 185396 = 1.02$$

Forces in pier 2 using Model F

First-mode vibration period

For Model F, considering the translational spring support at the pier top in the model second component, k is calculated using Eq. (11).

$$k = \frac{K_{iso,2} H^3}{0.7 E_c I_{g,2}} = \frac{31867 \times 17.5^3}{1.529 \times 10^9} = 0.112$$

The frequency parameter λ_1 can be obtained by solving Eq. (10) or directly from Fig.3.

$$\lambda_1 = 1.892$$

The first vibration period of pier 2 shown in Table 2 and the acceleration spectrum value are obtained as follows.

$$T_{P2} = 0.153\,s \text{ and } S(T_{P2}) = 0.848g$$

Mode shape and modal participation factor

The pier is also divided into 20 elements and the modal coordinates for each node are computed from Eq. (12).

$$\{\phi_1\}^T = \{0.0030, 0.0265, 0.0718, 0.1372, 0.2211, 0.3219, 0.4377, 0.5671, 0.7083, 0.8600, 1.0205, 1.1884, 1.3625, 1.5415, 1.7241, 1.9095, 2.0968, 2.2851, 2.4741, 2.6632\}$$

And the modal participation factor is:.

$$\gamma_1 = 0.568$$

Pier shear and moment distribution:

The nodal inertia forces along the pier heights are computed from:

$$\{V_{P2}\}^T_{(kN)} = \gamma_1 S_a(T_{P2})[M]\{\phi_1\} = \{2, 13, 37, 70, 113, 164, 223, 289, 361, 438, 520, 606, 695, 786, 879, 973, 1069, 1165, 1261, 1357\}$$

and the resulting shears and bending moments are given in Fig. 19.

The pier base shear and moment are $V_{P2}{}^{p} = 11020\,kN$ and $M_{P2}{}^{p} = 139990\,kN.m$, respectively. According to Table 2, the base shear and moment of the superstructure component are $V_{P2}{}^{ss} = 7223\,kN$ and $M_{P2}{}^{ss} = 126400\,kN.m$, respectively. Then, the designed base shear and moment of Model F shown in Table 2 (as noted by the *"F"* superscript) are computed as follows.

$$V_{P2}^{F} = \sqrt{(V_{P2}{}^{ss})^2 + (V_{P2}{}^{p})^2} = \sqrt{7223^2 + 11020^2} = 13176\,kN \qquad \text{(see Table 2)}$$

$$M_{P2}^{F} = \sqrt{(M_{P2}{}^{ss})^2 + (M_{P2}{}^{p})^2} = \sqrt{126400^2 + 139990^2} = 188610\,kN.m \qquad \text{(see Table 2)}$$

Finally, the accuracies of the base shear and moment shown in Fig. 7 are:

$$V_{P2}^{F} / V_{P2}^{MMSA} = 13176 / 13350 = 0.99$$

$$M_{P2}^{F} / M_{P2}^{MMSA} = 188610 / 185396 = 1.02$$

Table-1-Word Click here to download Table Table 1.docx

Table 1. Main parameters of the bridge model in Fig. 4

Components	Properties (units)	Values
Superstructure	Mass of superstructure, M_{ss} (tons)	19310
Piers	Mass of pier 1, $M_{p,1}$ (tons)	1728
	Mass of pier 2, $M_{p,2}$ (tons)	2160
	Total mass of piers, M_p (tons)	7776
	Mass ratio M_p/M_{ss}	0.40
	Stiffness of pier 1, $k_{p,1}$ (kN/m)	438200
	Stiffness of pier 2, $k_{p,2}$ (kN/m)	855800
	Reaction force at pier 1, W_1 (kN)	11278
	Reaction force at pier 2, W_2 (kN)	83343
Isolators	Characteristic strength of isolator 1, μW_1 (kN)	338
	Post-yield stiffness of isolator 1, W_1/R (kN/m)	2820
	Characteristic strength of isolator 2, μW_2 (kN)	2500
	Post-yield stiffness of isolator 2, W_2/R (kN/m)	20836

Table-2-Word Click here to download Table Table 2.docx

Table 2. Results of the simplified models (Models A to F) and MMSA[a]

Responses	Model A	Model B	Model C	Model D	Model E [a]	Model F [a]	MMSA
$k_{iso,1}$ (kN/m)	4283	4270	4176	4270	4270	4270	/
$k_{iso,2}$ (kN/m)	31650	31867	31130	31867	31867	31867	/
$k_{eff,1}$ (kN/m)	4283	4229	4137	4229	4229	4229	/
$k_{eff,2}$ (kN/m)	31650	30723	30037	30723	30723	30723	/
T_{P1} (s)	/	/	/	0.227	0.198	0.197	0.197
T_{P2} (s)	/	/	/	0.179	0.155	0.153	0.154
K_{iso}/K_p	0.0278	0.0270	0.0264	0.0270	0.0270	0.0270	/
K_{eff} (kN/m)	71866	69904	68348	69904	69904	69904	/
ξ	21.8%	21.3%	20.3%	21.3%	21.3%	21.3%	/
T_{eff} (s)	3.255	3.302	3.555	3.302	3.302	3.302	3.309
D_{ss} (m)	0.231	0.235	0.252	0.235	0.235	0.235	0.237
V_{P1} (kN)	989	995	1041	5310	8909	8858	9314
V_{P2} (kN)	7311	7223	7561	9720	13168	13176	13350
M_{P1} (kN.m)	17314	17413	18224	92922	113987	113053	112872
M_{P2} (kN.m)	127946	126400	132319	170106	188544	188610	185396

[a] See detail in Appendix I.

Table 3. Accuracy of SM using Models B, E and F compared to MMSA[a]

Response	MMSA	Model B	Model E	Model F
Superstructure displacements (m)	0.122	0.131 (1.08)	0.131(1.08)	0.131 (1.08)
First vibration periods T_{eff} (s)	1.78	1.82 (1.02)	1.82 (1.02)	1.82 (1.02)
Second vibration periods T_{P1}[b] (s)	0.176	/	0.184 (1.04)	0.176 (1.00)
Third vibration periods T_{P2}[b] (s)	0.112	/	0.115 (1.02)	0.113 (1.00)
P1 base shears V_{P1} (kN)	3506	2119 (0.60)	3636 (1.04)	3584 (1.02)
P2 base shears V_{P2} (kN)	4182	2090 (0.50)	4461 (1.07)	4321 (1.03)
P1 base moments M_{P1} (kN.m)	34528	25429 (0.74)	35547 (1.03)	34959 (1.01)
P2 base moments M_{P2} (kN.m)	51051	33440 (0.66)	55115 (1.08)	52927 (1.04)

[a] Values in brackets correspond to ratios with respect to MMSA results.

[b] T_{p1}, and T_{p2} are the first-mode vibration periods for individual pier 1 and pier 2, respectively.

Table-4-Word Click here to download Table Table 4.docx

Table 4. Accuracy of SM using Model F and MMSA compared to NLTHA[a]

Responses	Model F	MMSA	NLTHA
D_{ss} (m)	0.138 (1.21)	0.139 (1.22)	0.114
V_{P1} (kN)	9593 (0.92)	9628 (0.92)	10421
V_{P2} (kN)	14488 (1.15)	14215 (1.13)	12546
M_{P1} (kN.m)	121997 (1.02)	121154 (1.02)	119045
M_{P2} (kN.m)	192757 (1.06)	189056 (1.04)	181131

[a] Ratios in brackets are obtained with respect to NLTHA results.

Figure Captions List

Fig. 1. Description of simplified models: (a) Model A (isolated superstructure only); (b) Model B (flexible massless piers); (c) Model C (flexible piers with lumped 1/3 piers mass at the superstructure level); and (d) Model D (two SDOF with lumped 1/3 pier mass at the tops of piers)

Fig. 2. Proposed simplified models: (a) Model E (superstructure SDOF system and flexible mass pier); (b) Model F (superstructure SDOF system and flexible piers with mass and top isolators)

Fig. 3. Frequency parameter λ_1 for the fundamental period

Fig. 4. Bridge model geometry, deck and pier cross section (all dimensions are in meters; longitudinal direction and transverse direction are the X-axes and the Y-axes, respectively)

Fig. 5. Force-displacement hysteresis loop for FPS bearings

Fig. 6. Design response spectra: (a) Composite acceleration spectrum and (b) Displacement spectrum

Fig. 7. Comparisons of normalized seismic responses of simplified models: (a) First periods, T_1 and superstructure displacements, D_{ss}; (b) Pier base shears, V_{P1}, and V_{P2}; and (c) Pier base moments, M_{P1}, and M_{P2}

Fig. 8. Comparisons of normalized seismic responses of Model A: (a) Superstructure displacements, D_{ss}; (b) First periods, T_1; (c)Base shears of pier 1, V_{P1}; (d) Base shears of pier 2, V_{P2}; (e) Base moments of pier 1, M_{P1}; and (f) Base moments of pier 2, M_{P2}

Fig. 9. Comparisons of normalized seismic responses of Model B: (a) Superstructure displacements, D_{ss}; (b) First periods, T_1; (c)Base shears of pier 1, V_{P1}; (d) Base shears of pier 2, V_{P2}; (e) Base moments of pier 1, M_{P1}; and (f) Base moments of pier 2, M_{P2}

Fig. 10. Comparisons of normalized seismic responses of Model C: (a) Superstructure displacements, D_{ss}; (b) First periods, T_1; (c)Base shears of pier 1, V_{P1}; (d) Base shears of pier 2, V_{P2}; (e) Base moments of pier 1, M_{P1}; and (f) Base moments of pier 2, M_{P2}

Fig. 11. Comparisons of normalized seismic responses of Model D: (a) Base shears of pier 1, V_{P1}; (b) Base shears of pier 2, V_{P2}; (c) Base moments of pier 1, M_{P1}; and (d) Base moments of pier 2, M_{P2}

Fig. 12. Comparisons of normalized seismic responses of Model E: (a) First periods of pier 1, T_{P1}; (b) First periods of pier 2, T_{P2}; (c) Base shears of pier 1, V_{P1}; (d) Base shears of pier 2, V_{P2}; (e) Base moments of pier 1, M_{P1}; and (f) Base moments of piers 2, M_{P2}

Fig. 13. Comparisons of normalized seismic responses of Model F: (a) First periods of pier 1, T_{P1}; (b) First periods of pier 2, T_{P2}; (c) Base shears of pier 1, V_{P1}; (d) Base shears of pier 2, V_{P2}; (e) Base moments of pier 1, M_{P1}; and (f) Base moments of pier 2, M_{P2}

Fig. 14. Bridge model geometry, deck and pier cross section (all dimensions are in meters)

Fig. 15. Bilinear force–deformation relationship of HDR

Fig. 16. Finite element model in SAP2000

Fig. 17. (a) Acceleration time history used in the nonlinear time history analyses and (b) Response spectrum

Fig. 18. Shear force and moment distributions of pier 2 calculated using Model E

Fig. 19. Shear force and moment distributions of pier 2 calculated using Model F

Click here to download Figure 03-Figure 1-YM-RT-PL-JL-2016-8-25.pdf

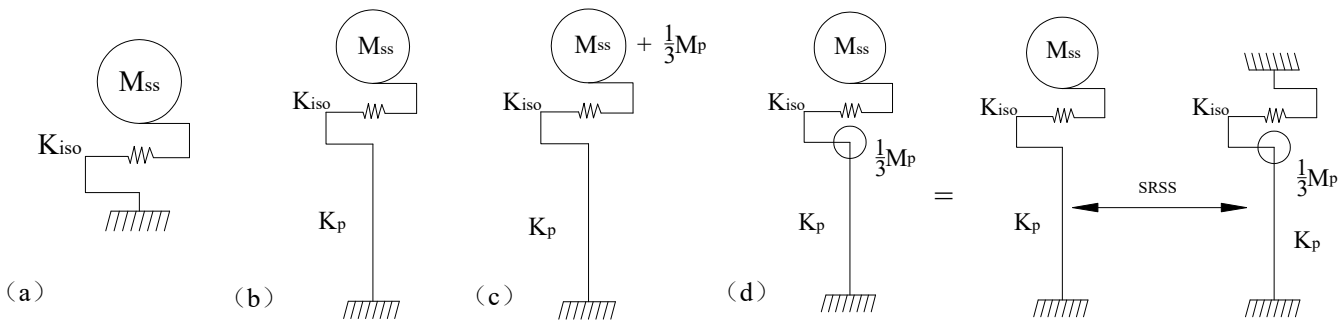

Click here to download Figure 04-Figure 2-YM-RT-PL-JL-2016-8-25.pdf

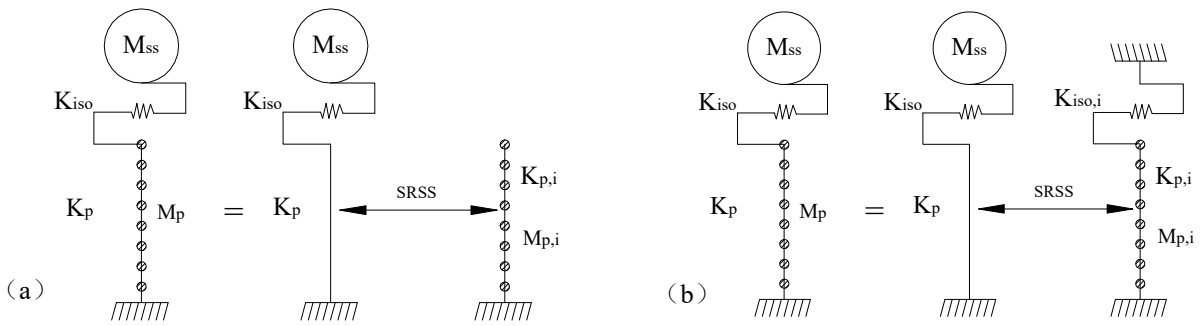

Click here to download Figure 05-Figure 3-YM-RT-PL-JL-2016-8-25.pdf

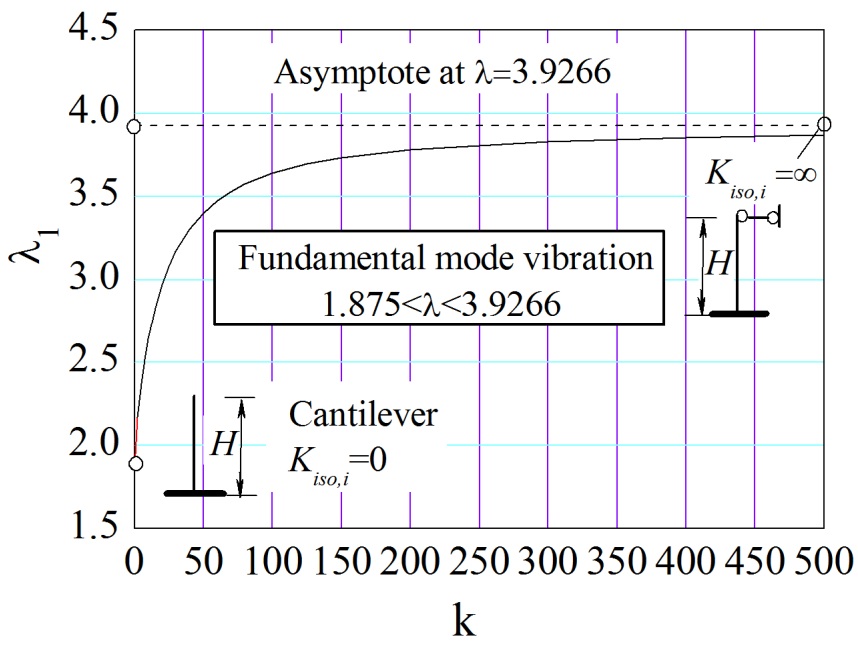

Click here to download Figure 06-Figure 4-YM-RT-PL-JL-2016-8-25.pdf

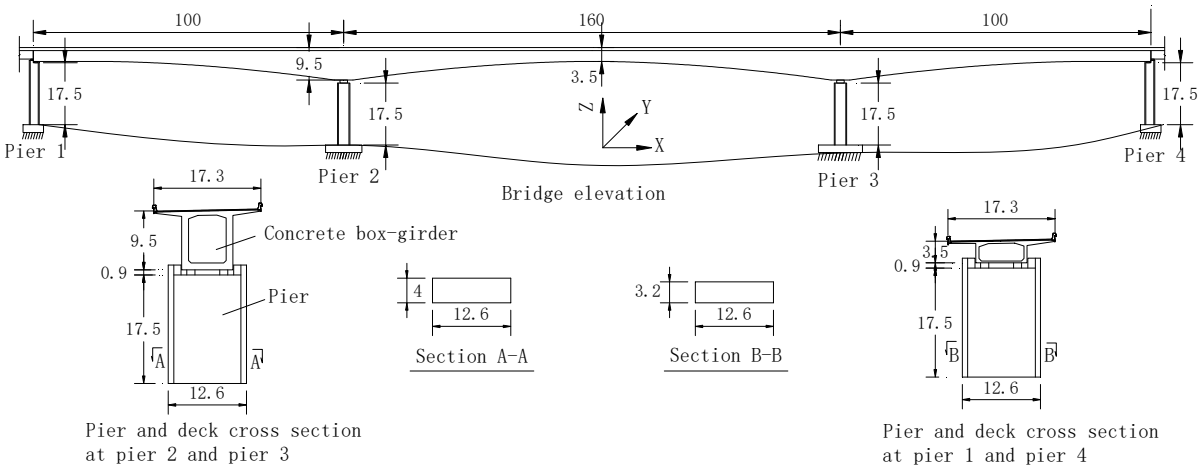

Click here to download Figure 07-Figure 5-YM-RT-PL-JL-2016-8-25.pdf

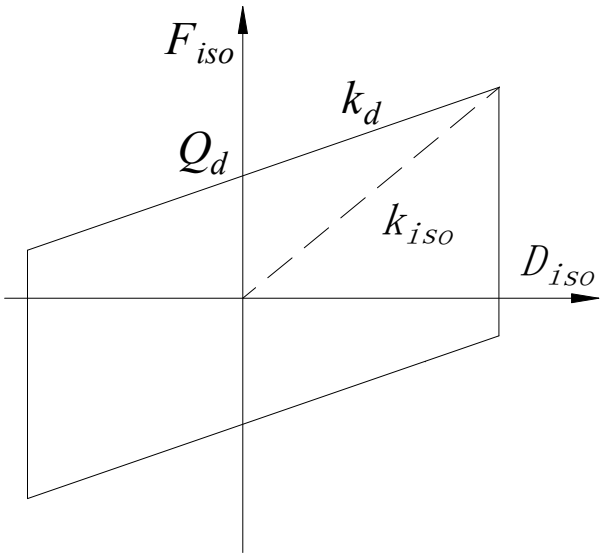

Click here to download Figure 08-Figure 6-YM-RT-PL-JL-2016-8-25.pdf

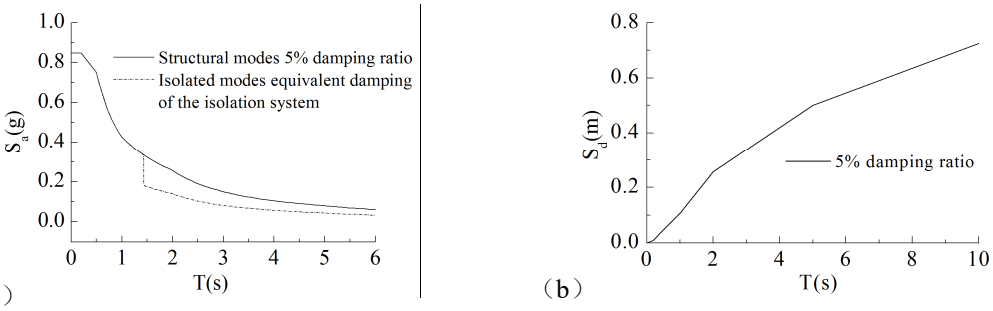

Click here to download Figure 09-Figure 7-YM-RT-PL-JL-2016-8-25.pdf

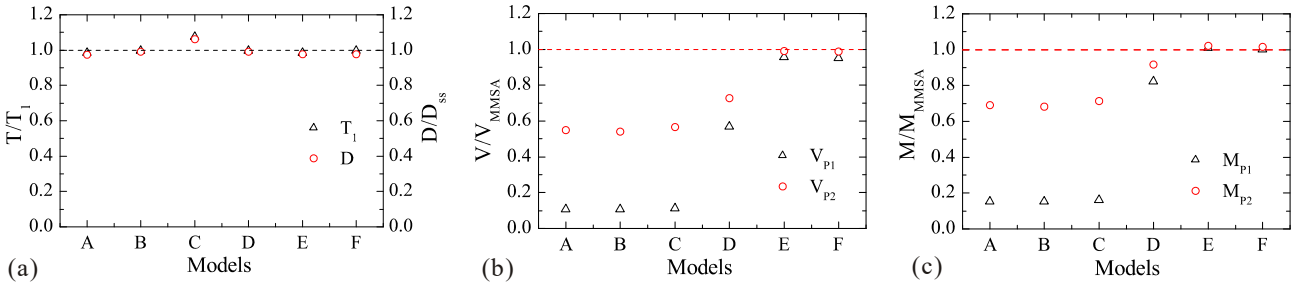

Click here to download Figure 10-Figure 8-YM-RT-PL-JL-2016-8-25.pdf

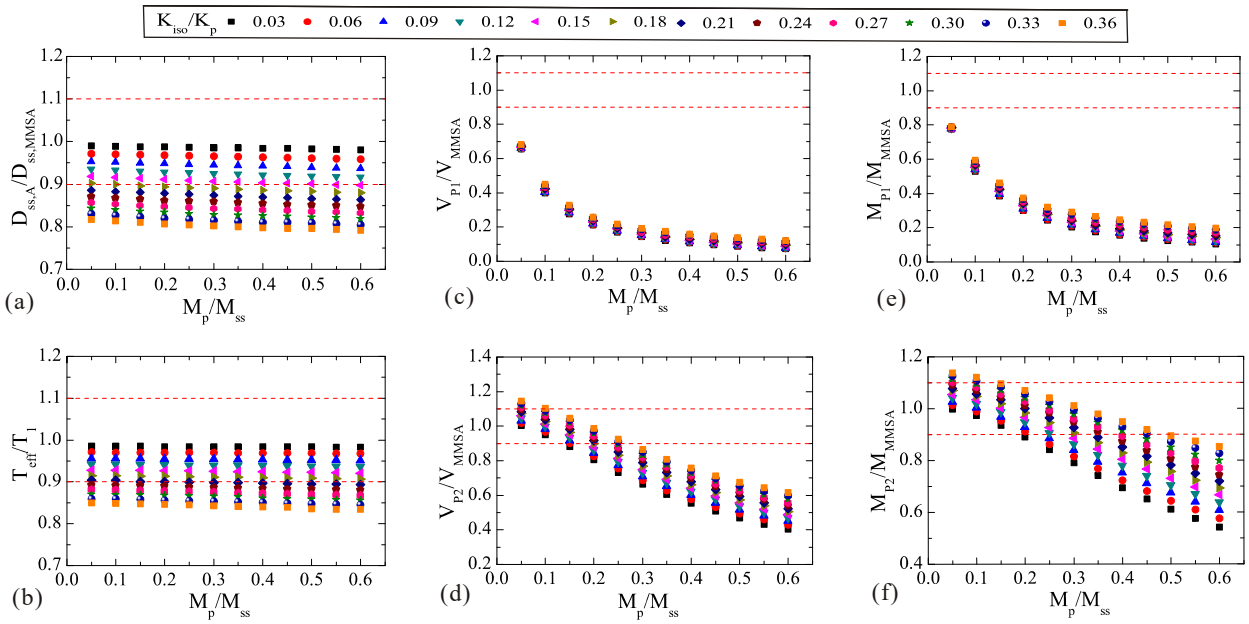

Click here to download Figure 11-Figure 9-YM-RT-PL-JL-2016-8-25.pdf

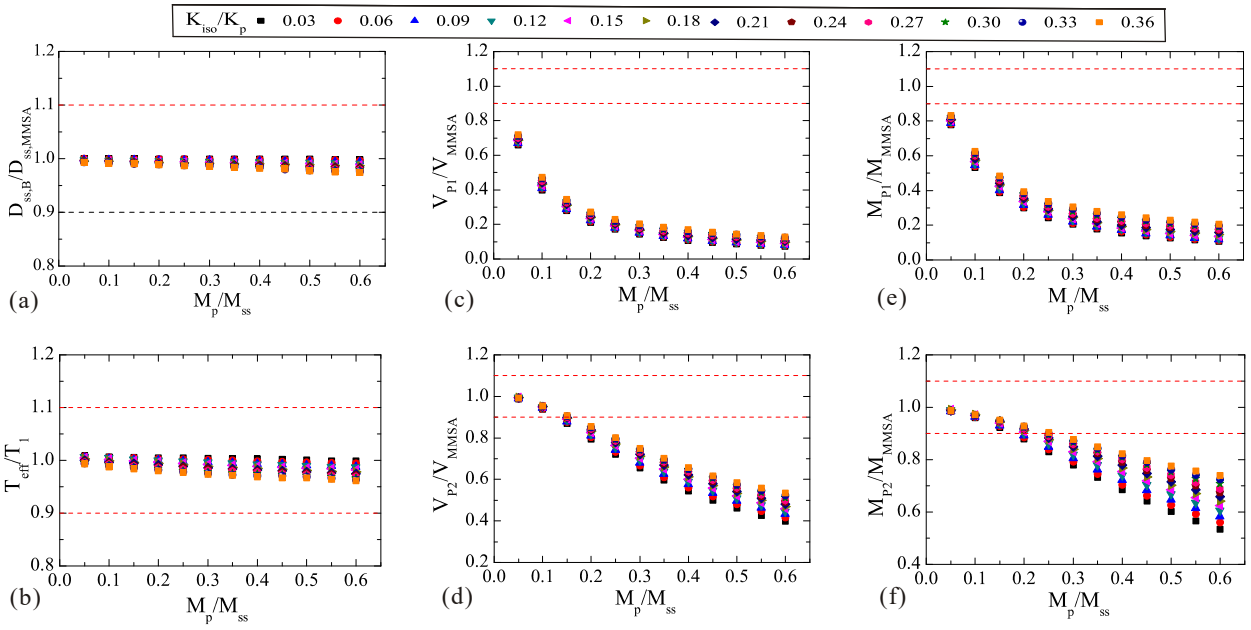

Click here to download Figure 12-Figure 10-YM-RT-PL-JL-2016-8-25.pdf

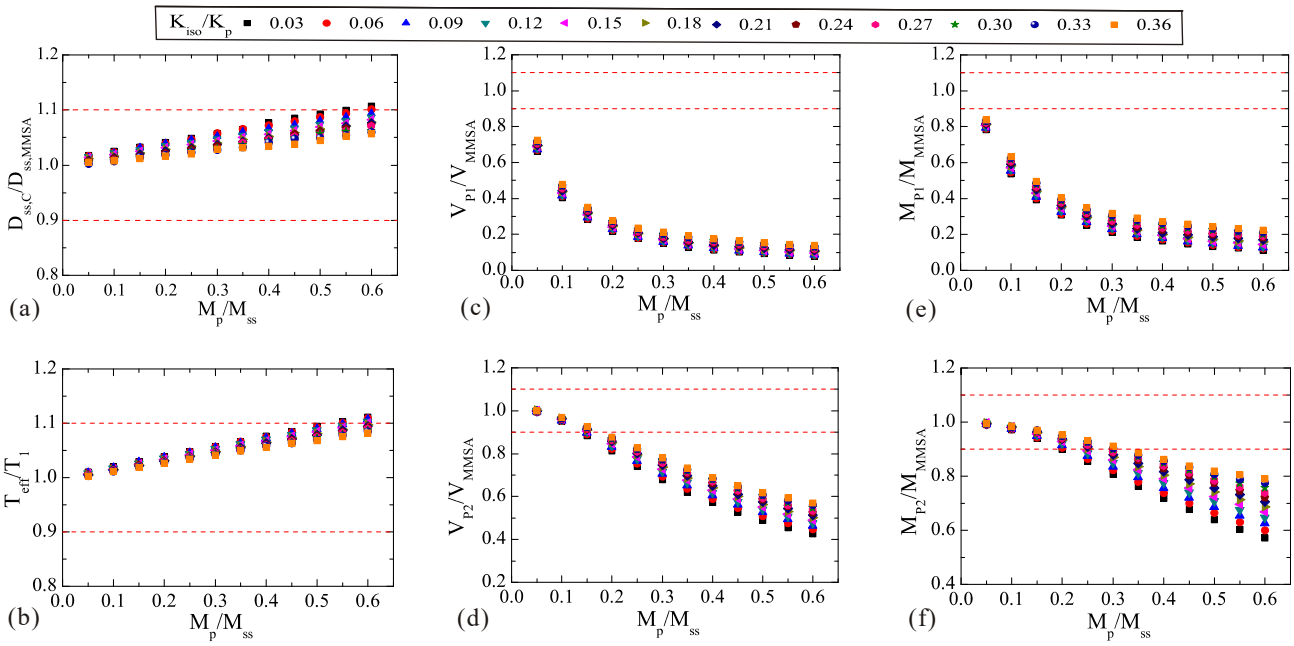

Click here to download Figure 13-Figure 11-YM-RT-PL-JL-2016-8-25.pdf

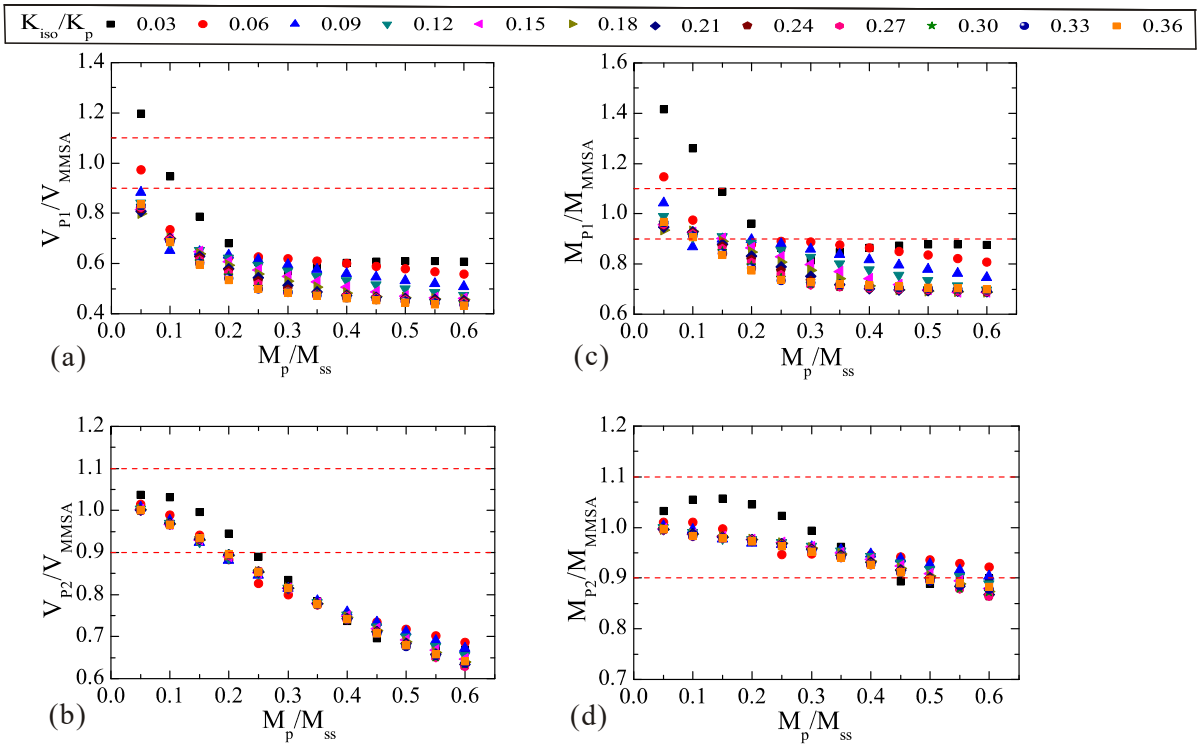

Click here to download Figure 14-Figure 12-YM-RT-PL-JL-2016-8-25.pdf

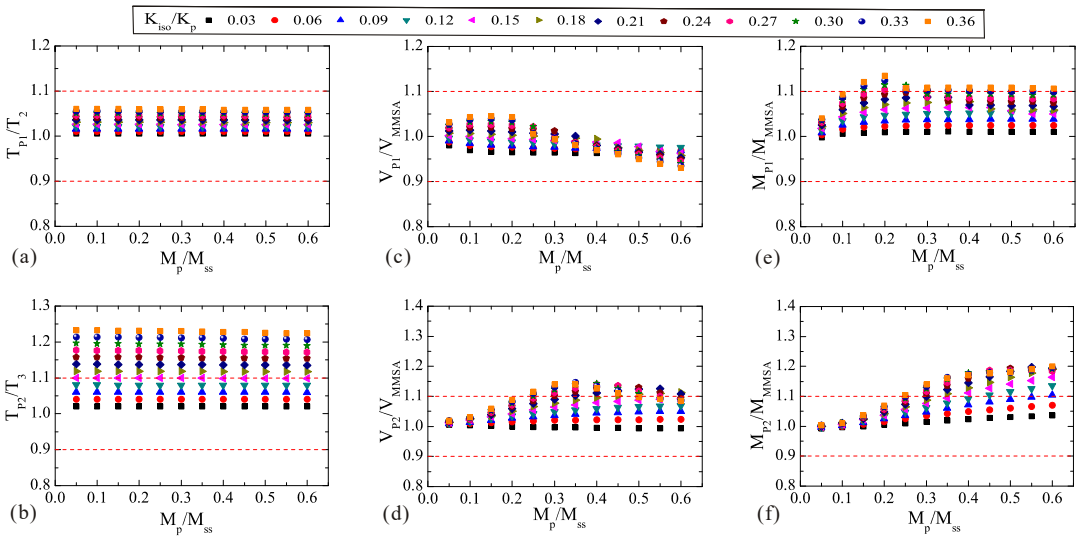

Click here to download Figure 15-Figure 13-YM-RT-PL-JL-2016-8-25.pdf

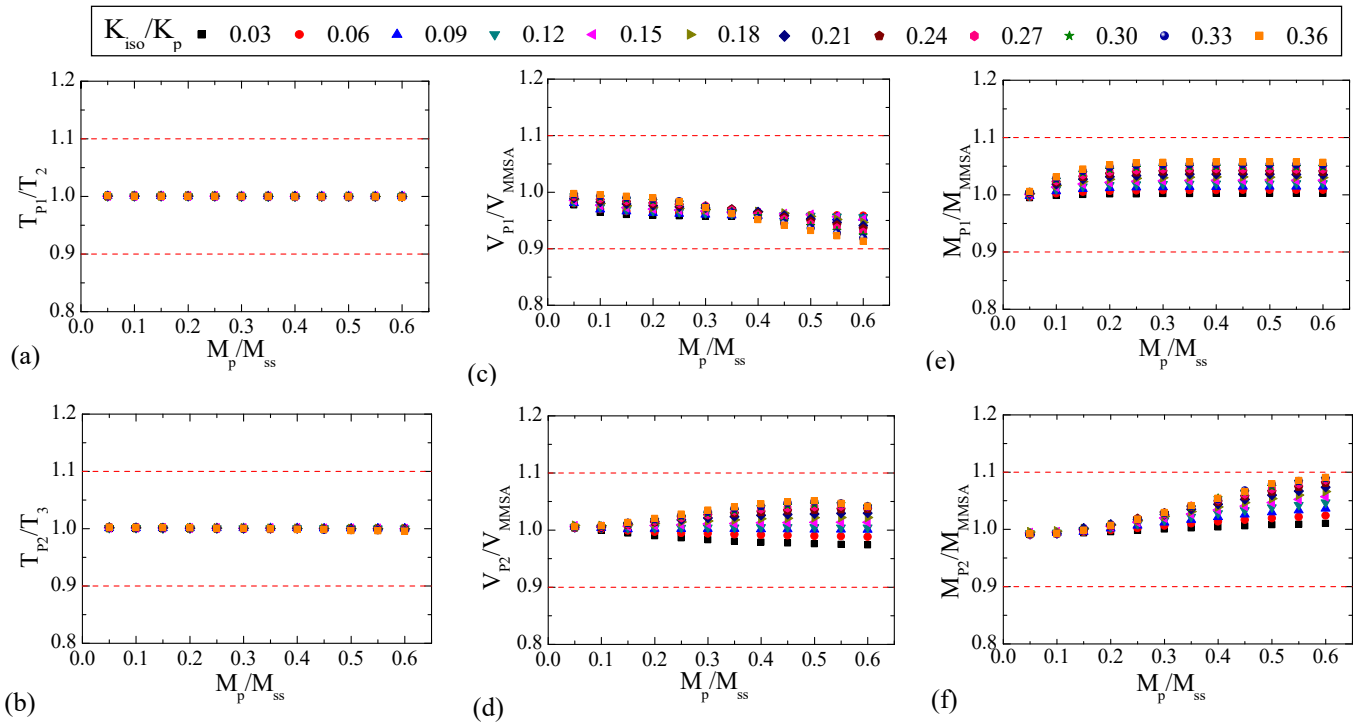

Click here to download Figure 16-Figure 14-YM-RT-PL-JL-2016-8-25.pdf

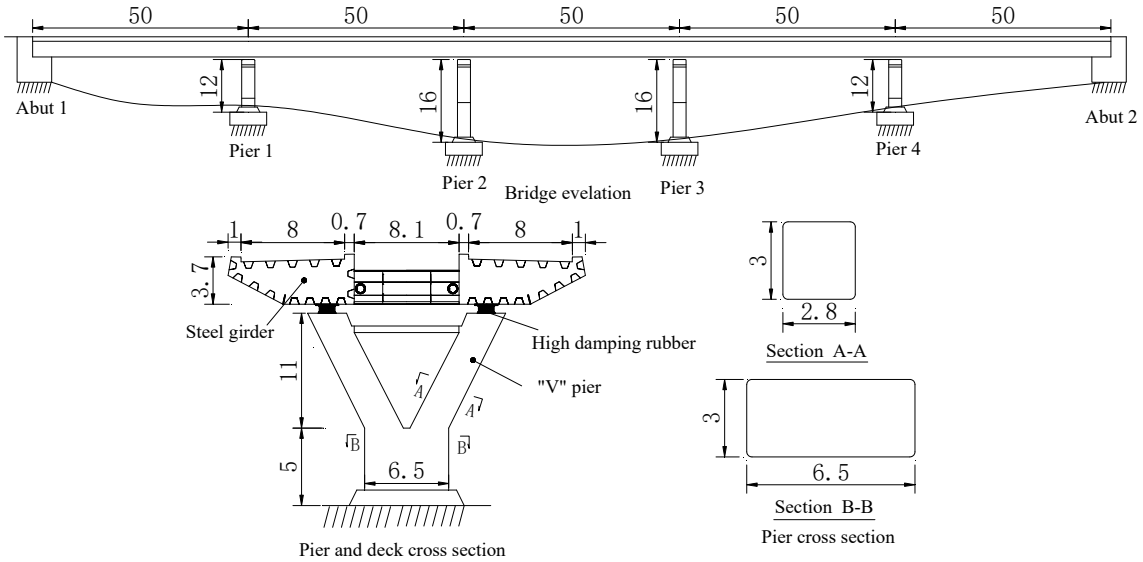

Click here to download Figure 17-Figure 15-YM-RT-PL-JL-2016-8-25.pdf

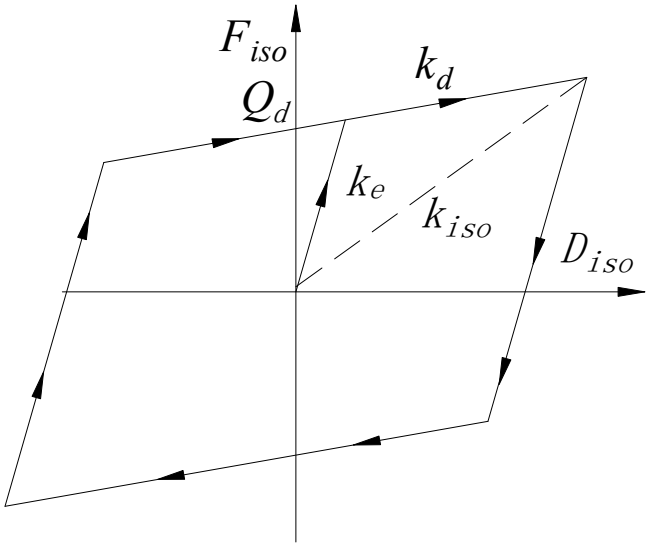

Click here to download Figure 18-Figure 16-YM-RT-PL-JL-2016-8-25.pdf

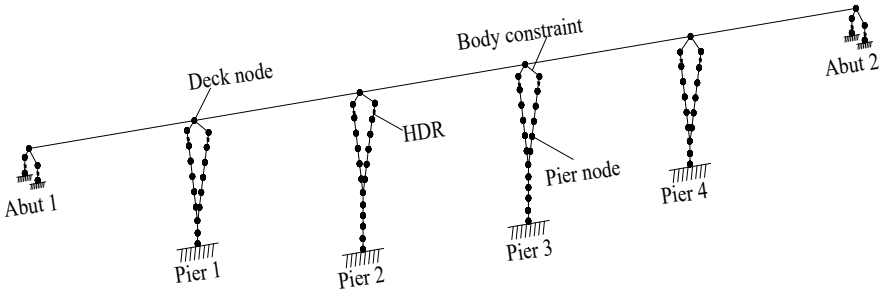

Click here to download Figure 19-Figure 17-YM-RT-PL-JL-2016-8-25.pdf

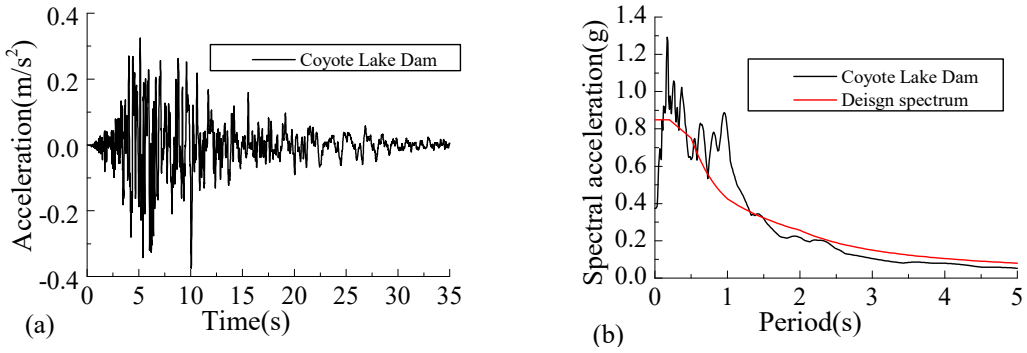

Click here to download Figure 20-Figure 18-YM-RT-PL-JL-2016-8-25.pdf

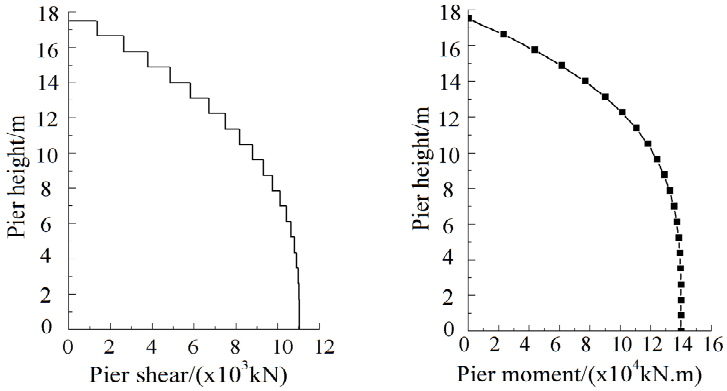
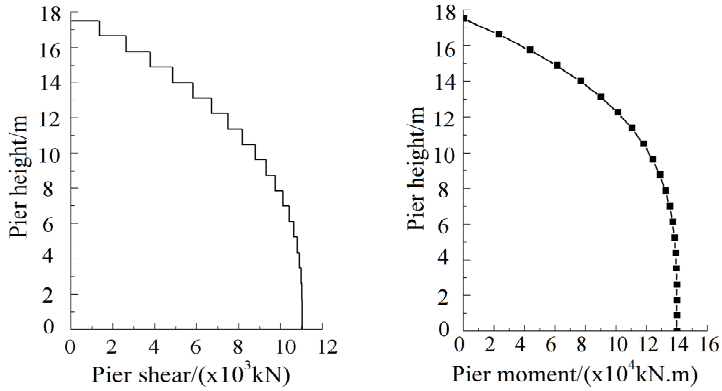
Click here to download Figure 21-Figure 19-YM-RT-PL-JL-2016-8-25.pdf